



# Dwarf Irregular Galaxy Leo A. II. Suprime-Cam $R$ and $H\alpha$ Stellar Photometry

Rima Stonkutė<sup>1</sup> and Vidas Vansevicius<sup>1</sup>Center for Physical Sciences and Technology, Saulėtekio av. 3, 10257 Vilnius, Lithuania; [rima.stonkute@ftmc.lt](mailto:rima.stonkute@ftmc.lt)

Received 2021 October 28; revised 2022 January 23; accepted 2022 January 28; published 2022 February 23

## Abstract

We have surveyed the complete extent of Leo A, which is an apparently isolated Local Group dwarf irregular galaxy, in  $B$ ,  $V$ ,  $R$ ,  $I$  (the Johnson–Cousins system), and  $NA656$  (centered on  $H\alpha$ ) passbands with the Subaru Telescope equipped with the Suprime-Cam mosaic camera.  $B$ ,  $V$ , and  $I$  photometry results were published earlier by Stonkutė et al. The recently published Stetson’s high-quality photometric standards in the  $R$  passband encouraged us to calibrate and make available to the community deep ( $R \sim 25$  mag)  $R$  and  $NA656$  photometry results in the field of Leo A ( $20' \times 24'$ ). We present the photometry catalog of 28,224 objects in  $R$  and 25,800 objects in  $NA656$  passbands. This catalog could serve for future imaging and spectroscopic observation programs of Leo A, especially targeted to study emission-line objects. Also, we demonstrate the capability of the  $B$ ,  $V$ ,  $R$ , and  $NA656$  passband system to separate Milky Way M-type dwarfs and late-type evolved stars in external galaxies, as well as to recognize early-type (Be, B[e]) emission-line stars.

*Unified Astronomy Thesaurus concepts:* Dwarf irregular galaxies (417); Stellar photometry (1620); Catalogs (205); Galaxies (573); Dwarf galaxies (416)

*Supporting material:* machine-readable table

## 1. Introduction

Leo A (DDO 69) is a well-isolated dwarf irregular galaxy in the Local Group, at a distance of  $\sim 820$  kpc; see Leščiņskaitė et al. (2021) and references therein for other parameters. This low-mass, dark-matter-dominated (Brown et al. 2007), gas-rich (Hunter et al. 2012), and metal-poor galaxy (Kirby et al. 2017) contains multiple stellar populations covering a broad range of ages: H II regions trace recent star-forming activity, while RR Lyrae stars (Dolphin et al. 2002) indicate the existence of an ancient ( $\gtrsim 10$  Gyr) stellar population. Leo A is unique in a sense that it has a significantly delayed star formation (Cole et al. 2007), which is unlikely to have been triggered by external processes due to its isolation. Therefore, a well-calibrated stellar photometry catalog in five passbands will be useful for further studies of this remarkable galaxy.

Below we briefly mention the basic Suprime-Cam data reduction and stellar photometry procedures as they are identical to the ones described by Stonkutė et al. (2014). Then we discuss in more detail calibration issues and new photometry results.

The paper is organized as follows. In Section 2, we describe observations and data reduction procedures. Photometry and calibration procedures are described in Section 3. Results are discussed in Section 4. Conclusions are given in Section 5.

## 2. Observations and Data Reduction

Taking into account the angular size of Leo A ( $16'–20'$ ; Vansevicius et al. 2004; Stonkutė et al. 2018), the Subaru Telescope, equipped with the Prime Focus Camera (Suprime-Cam; Miyazaki et al. 2002), is ideally suited to study the stellar content down to  $R \sim 25$  mag at the galaxy’s very outskirts. A single exposure of the Suprime-Cam mosaic ( $5 \times 2$  MIT/LL  $2048 \times 4096$  CCD chips) covers a field of  $34' \times 27'$  (scale  $0''.2/\text{pixel}$ ).


Images of Leo A were acquired on 2002 November 4 (P.I. Nobuo Arimoto) through the broadband  $R$  (the Johnson–Cousins system) and the narrow nonstandard passband  $NA656$  filters<sup>1</sup> (hereinafter for brevity we mark this passband as  $NA$ ). The central wavelength of this passband is  $6566 \text{ \AA}$ , which approximately coincides with  $H\alpha$ ; the FWHM of the filter’s transmission curve is  $140 \text{ \AA}$ .

Observations were performed with a clear sky and good seeing conditions, and an FWHM of stellar images  $0''.6–0''.8$ . The telescope was dithered between exposures to avoid gaps amid CCDs while mapping the field. Five exposures in the  $R$  passband of 240 s each and five exposures in the  $NA$  passband of 540 s each were obtained.

Due to the noticeable gradient of the point-spread function (PSF) at the Suprime-Cam mosaic corners, for analysis, we used only six central CCDs ( $20' \times 24'$ ) comfortably covering the whole extent of Leo A. The survey field is centered at  $\alpha = 9^{\text{h}}59^{\text{m}}26^{\text{s}}.0$ ,  $\delta = +30^{\circ}46'50''.0$  (J2000), namely, slightly above the center of Leo A. All image reduction, object detection, and coordinate determination procedures were performed exactly as described in Stonkutė et al. (2014).

## 3. Photometry and Calibration

The stellar photometry was performed on the individual flat-fielded CCD frames by applying DAOPHOT (Stetson 1987) implemented in the IRAF software package (Tody 1993). The PSF photometry was performed with the `allstar` program by using PSF stars (typically  $\sim 30$ ) distributed uniformly across each CCD frame. We measured PSF magnitudes using apertures of a  $1.75 \times \text{FWHM}$  radius. Aperture corrections were derived by using apertures of a  $3.5 \times \text{FWHM}$  radius. We note that residual aperture corrections, used to transform magnitudes measured through the aperture of a  $3.5 \times \text{FWHM}$  radius to the total magnitudes, are constant for individual exposures on each CCD and were taken into account as zero-point offsets. For  $R$  and  $NA$

 Original content from this work may be used under the terms of the [Creative Commons Attribution 4.0 licence](https://creativecommons.org/licenses/by/4.0/). Any further distribution of this work must maintain attribution to the author(s) and the title of the work, journal citation and DOI.

<sup>1</sup> <https://www.subarutelescope.org/Observing/Instruments/SCam>

passbands we derived global photometric solutions of instrumental magnitudes over the whole survey field by applying aperture corrections and zero-points of individual frames via overlapping dithered frames. The final instrumental magnitudes were calculated by taking median values of the zero-point-corrected magnitudes measured in individual exposures. Additionally, for  $R$  and  $NA$  passbands, we checked the consistency of the photometry zero-points among individual CCDs and found the largest difference to be  $0.006 \pm 0.022$ , which we consider insignificant, accounting for the accuracy of the presented photometry data. More technical details on the PSF photometry procedures are provided in Stonkutė et al. (2014).

The list of objects measured in the  $R$  passband was merged by positional coincidence, adopting the maximum allowed coordinate difference of two pixels ( $0''.4$ ), with the objects from the catalog by Stonkutė et al. (2014). Therefore, only objects that have counterparts in the published catalog were introduced into the final catalog presented in this paper. In the Subaru Suprime-Cam  $B$ ,  $V$ , and  $I$  photometry catalog (Stonkutė et al. 2014) there are 38,856 objects, and in this paper we supplemented it with the photometry in the  $R$  passband for 28,224 objects. Additionally, photometry results in the  $NA$  passband for 25,800 objects that have counterparts among the  $R$  passband objects are also provided.

To transform instrumental  $R$  magnitudes to the standard photometric system, we used Stetson’s (ST) CCD standard stars (Stetson 2000; Stetson et al. 2019). From the ST standard stars catalog (Stetson Homogeneous photometry database<sup>2</sup>) we employed  $R$  and  $I$  passbands (the Johnson–Cousins system) for the calibration of the Suprime-Cam photometry. We used ST standard stars from the field centered on the Leo A galaxy (last modified on 2021 June 24).

We cross identified the ST catalog of standard stars with reliably measured stars from our catalog, allowing a maximum coordinate mismatch of  $0''.4$ . This resulted in 81 photometric standards. The standard stars ( $R \sim 19.3$ – $21.3$ ) are widely distributed across the Subaru Suprime-Cam survey field and span a sufficiently wide color range ( $R - I \sim -0.1$ – $2.2$ ) required for an accurate calibration.

The following three calibration equations were derived to transform instrumental ( $R_{\text{instr}} - I$ ) color indices to the standard photometric system:

$$R - I = (2.434 \pm 0.034) + (1.030 \pm 0.010) \times (R_{\text{instr}} - I) \quad (1)$$

in the cases of  $(R - I)_{\text{ST}} \leq 0.45$ ;

$$R - I = (2.160 \pm 0.066) + (0.888 \pm 0.043) \times (R_{\text{instr}} - I) \quad (2)$$

in the cases of  $0.45 < (R - I)_{\text{ST}} < 0.98$ ;

$$R - I = (2.529 \pm 0.022) + (1.167 \pm 0.025) \times (R_{\text{instr}} - I) \quad (3)$$

in the cases of  $(R - I)_{\text{ST}} \geq 0.98$ .

The differences  $(R - I) - (R - I)_{\text{ST}}$  of color indices are plotted versus  $R - I$  in Figure 1, where 81 ST standard stars are shown (the rms of color index differences is 0.027 mag). Therefore, calibrated photometric measurements in the  $R$  passband of 28,224 objects in total are supplemented to the former  $B$ ,  $V$ , and  $I$  measurements by Stonkutė et al. (2014).

To calibrate the  $NA$  passband, we used 856 starlike objects brighter than  $R = 22$  mag and their counterparts measured in

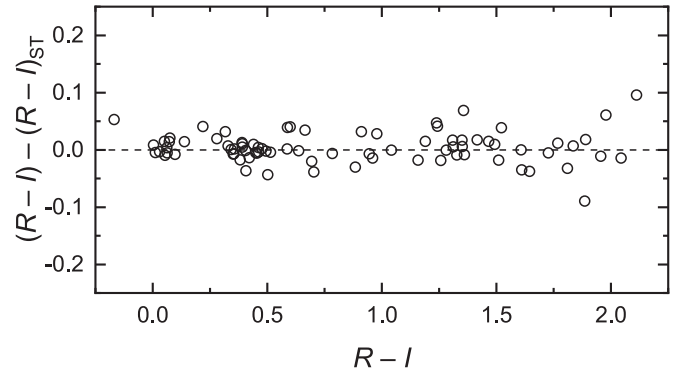


**Figure 1.** Color index differences of the 81 ST standards used for the  $R$  passband photometry calibration,  $(R - I) - (R - I)_{\text{ST}}$ , vs. the calibrated  $(R - I)$  color index. The rms of color index differences is 0.027 mag.

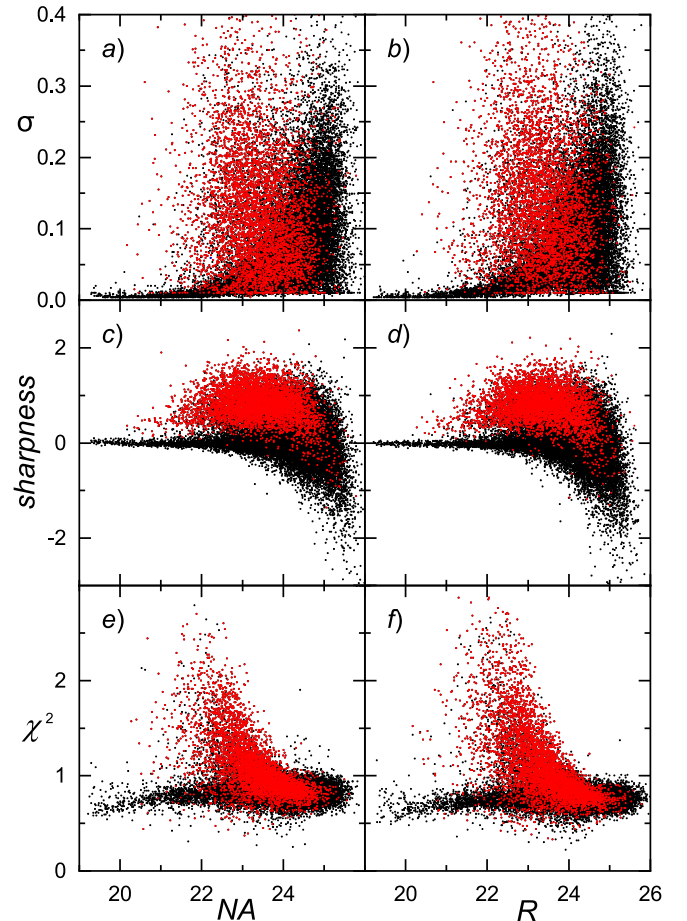


**Figure 2.** Photometry parameters for objects in the Leo A field; starlike and extended objects are indicated by black and red dots, respectively. Photometry quality parameters are plotted vs.  $R$  (22,944 starlike and 5280 extended objects) and vs.  $NA$  (21,036 and 4764, respectively) magnitudes in panels: (a), (b) the photometric errors,  $\sigma$ ; (c), (d) the object-profile sharpness in respect to the PSF, sharpness; (e), (f) the accuracy of object-profile fitting with the PSF,  $\chi^2$ .

the  $NA$  passband. The histogram’s maximum of the instrumental color index differences was determined based on 572 stars ( $\sigma_{NA} < 0.015$ ) at  $(NA - R)_{\text{instr}} = 1.417 \pm 0.009$ . Therefore, a correction of 1.417 was applied to calculate the final color indices  $NA - R = (NA - R)_{\text{instr}} - 1.417$ , which are further used in the paper.

To give an idea of the photometry quality, in Figure 2 we plot the following parameters: photometric errors,  $\sigma$ ; the object-

<sup>2</sup> <https://www.canfar.net/storage/vault/list/STETSON/homogeneous>

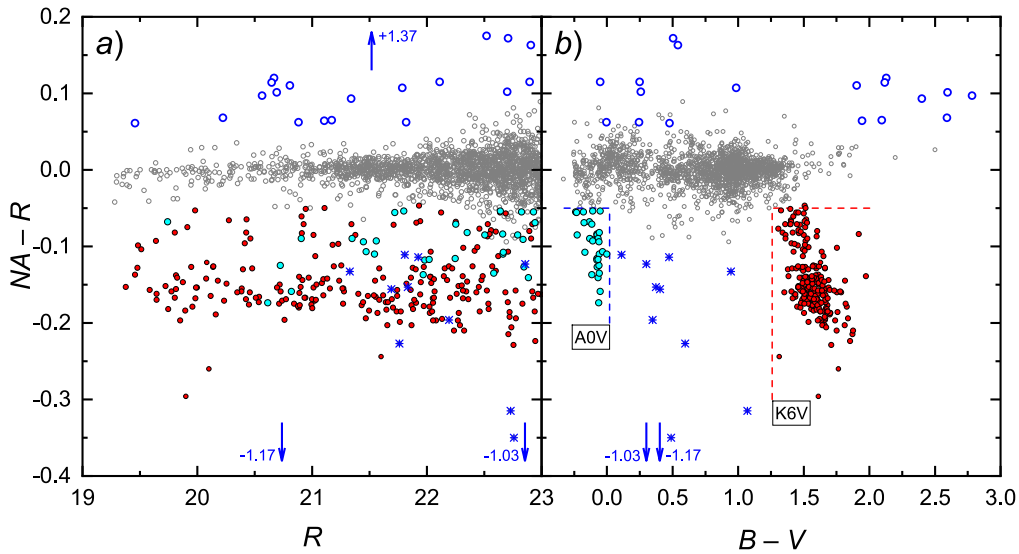


**Figure 3.** The  $NA-R$  color index vs.  $R$  magnitude (a) and vs.  $B-V$  color index (b) of the bright ( $R < 23$ ) starlike objects in the Leo A field plotted as gray dots. Two groups of stars with flux excesses ( $NA-R < -0.05$ ) in the  $NA$  passband are overplotted: the Milky Way late-type stars (red dots) and the early-type emission-line stars (cyan dots). Dashed red and dashed blue lines show the regions occupied by the solar metallicity stars of spectral types later than K6V and earlier than A0V, respectively (Pecaut & Mamajek 2013). Blue dots mark objects with a significant flux excess in the  $NA$  passband that do not belong to the previous two groups of stars (red and cyan dots). Blue open circles mark stars with a significant flux deficit in the  $NA$  passband. Blue arrows mark objects beyond the limits of the figure; numbers adjacent to arrows indicate values of their  $NA-R$  color index.

**Table 1**  
The Suprime-cam Photometry Catalog in the Leo A Field

ID	$\alpha_{J2000}^a$	$\delta_{J2000}^a$	$V$	$B-V$	$V-I$	$R$	$NA-R$	$R-I$	$\sigma_R^b$	$\sigma_{NA-R}^b$	$n_R^c$	$n_{NA}^c$	Type <sup>d</sup>
J095839.45+305247.5	149.6644	+30.8799	24.486	0.400	0.449	24.103	...	0.066	0.040	...	2	...	0
J095839.57+304340.5	149.6649	+30.7279	21.602	1.603	2.672	20.540	-0.173	1.610	0.010	0.014	2	2	2
J095839.58+304230.3	149.6649	+30.7084	24.160	0.375	0.732	23.821	-0.089	0.393	0.221	0.361	2	2	1

#### Notes.

<sup>a</sup> Equatorial coordinates (degrees) in the USNO-B1.0 catalog system.

<sup>b</sup> Photometric errors:  $\sigma_R, \sigma_{NA-R} = (\sigma_{NA}^2 + \sigma_R^2)^{1/2}$ .

<sup>c</sup> The number of individual measurements in  $R$  and  $NA$  passbands;  $2 \leq n \leq 5$ .

<sup>d</sup> Object types: 0–starlike; 1–extended (Stonkutė et al. 2014); 2–bright ( $R < 23$  mag) starlike, plotted in Figures 3–5.

(This table is available in its entirety in machine-readable form.)

profile sharpness in respect to the PSF,  $sharpness$ ; and the object-profile fitting accuracy with the PSF,  $\chi^2$ ; versus  $NA$  and  $R$  magnitudes. The parameters  $sharpness$  and  $\chi^2$  are defined in Stetson et al. (2019) and are widely discussed by Stetson & Harris (1988). Bright extended sources (red dots) can be clearly distinguished in the parameter space and the majority of them have  $sharpness \gtrsim 0.5$  and  $\chi^2 \gtrsim 1$ .

## 4. Results and Discussion

The Suprime-Cam photometry catalog of 28,224 objects ( $R \sim 19-26$  mag) in the Leo A field ( $20' \times 24'$ ) centered at  $\alpha = 9^h59^m26^s.0$ ,  $\delta = +30^\circ46'50''.0$  is presented in Table 1. Object coordinates,  $V$  and  $R$  magnitudes,  $B-V$ ,  $R-I$ ,  $V-I$ , and  $NA-R$  color indices, as well as photometric errors  $\sigma_R$ ,  $\sigma_{NA-R}$ , and the number of independent measurements of the  $R$  and  $NA$  magnitudes are provided. The  $V$  magnitude and  $B-V$  and  $V-I$  color indices are given for convenience from Stonkutė et al. (2014). The catalog contains 22,944 starlike and 5280 extended objects. Photometry results in the  $NA$  passband are provided for 21,036 starlike and 4764 extended objects. The objects were classified based on the PSF fitting parameters ( $sharpness$

and  $\chi^2$ ) and the interactive visual one-by-one inspection of the objects in combined multicolor images by Stonkutė et al. (2014).

To demonstrate the quality of photometry and the power of the  $NA-R$  color index for peculiar star recognition and classification, we selected a sample of bright ( $R < 23$  mag) starlike objects (Table 1; Type = 0). The steps of further object-list rectification were the following: (i) removal of objects with deviating  $sharpness$  and  $\chi^2$  parameters according to the recipe by Leščinskaitė et al. (2021); (ii) application of sharpness limits,  $sharpness_R \leq 0.3$  and  $sharpness_{NA} \leq 0.3$ ; and (iii) removal of stellar blends in the Suprime-Cam frames based on a careful visual inspection performed on the  $R$  passband Suprime-Cam frames and the Hubble Space Telescope (HST) Advanced Camera for Surveys frames from the HST program 10,590. The final list of 2008 starlike objects was used to plot Figures 3–5. These objects in Table 1 are marked as Type = 2.

For the analysis we used two diagrams (Figure 3): the  $NA-R$  color index versus the  $R$  magnitude (panel (a)) and versus the color index  $B-V$  (panel (b)). We considered values ( $|NA-R| \gtrsim 0.05$ ) of the color index  $NA-R$  as indicators of star peculiarity. These limits of  $NA-R$  are well above the

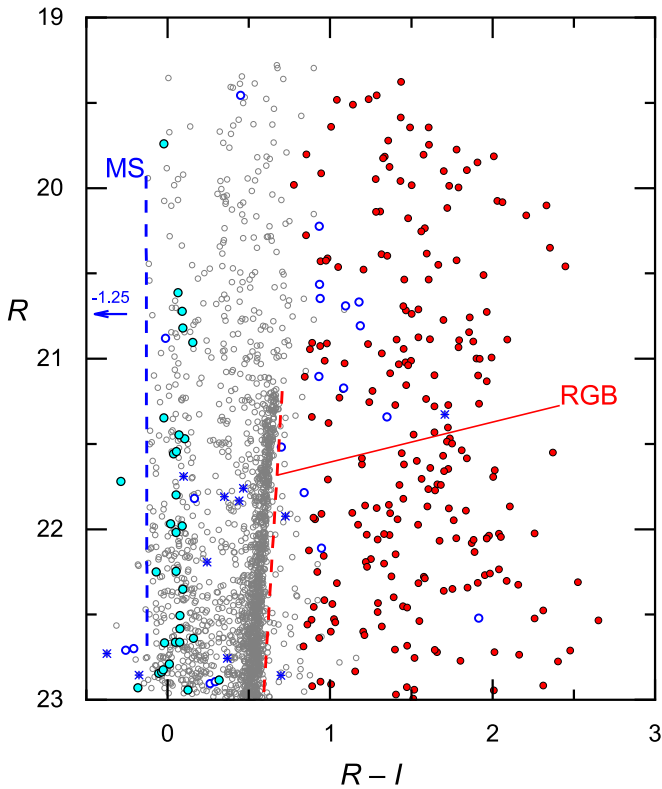


**Figure 4.** The  $R$  magnitude vs.  $R-I$  of 2008 bright starlike objects in the Leo A field. Symbols mark the same types of objects as in Figure 3. A blue arrow marks an object beyond the limits of the figure; a number adjacent to the arrow indicates the value of the  $R-I$  color index. The blue dashed line marks the main sequence (MS) and the red dashed line marks the red giant branch (RGB) of the Leo A galaxy.

photometric errors; therefore, these stars possess some kind of peculiarities in their spectra within the range of  $NA$  (140 Å).

Two groups of stars possessing significant flux excesses ( $NA - R \lesssim -0.05$ ) in the  $NA$  passband could be easily recognized in Figure 3(b): 226 M-type dwarfs of the Milky Way (red dots) and 31 Be-type (or B[e]) emission-line stars of Leo A (cyan dots). These groups are marked with the dashed red and dashed blue lines, indicating regions occupied by the solar metallicity stars of spectral types later than K6V and earlier than A0V, respectively (Pecaut & Mamajek 2013).

To reliably separate M-type Milky Way dwarfs from the late-type evolved stars residing in nearby galaxies is of high importance for stellar population studies (Leščinskaitė et al. 2021). The color-magnitude diagram (Figure 4) illustrates the complexity of this problem and demonstrates that the method based on the  $NA$  passband is performing well. Recognized Milky Way M-type dwarfs are distributed evenly across the field (Figure 5), which supports their classification as foreground stars.

On the other hand, blue open circles in Figure 3 mark 20 stars with a flux deficit in the  $NA$  passband. The majority (12) of these objects are late-type AGB stars in Leo A (Leščinskaitė et al. 2021). Peculiarities of other objects (eight) are of an unidentified origin. It is worth noting that this group (blue open circles in Figures 3–5) contains eight previously known variable stars. Therefore, the method to separate the Milky Way M-type dwarfs from the late-type evolved stars (Figure 3) can be applied to clean out samples of late-type stars in nearby galaxies from the foreground objects; this is especially

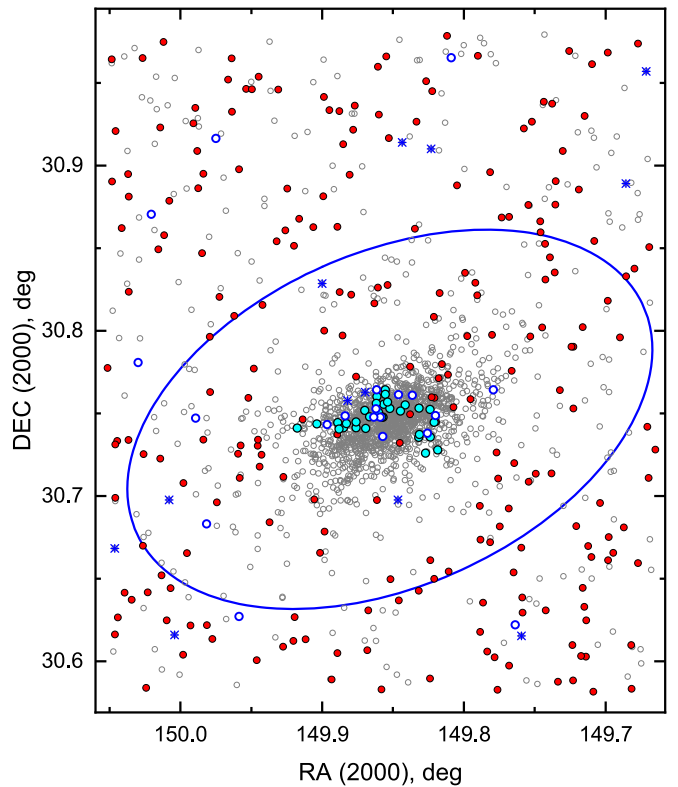


**Figure 5.** A spatial distribution of 2008 bright starlike objects in the Leo A field ( $R < 23$  mag). Symbols mark the same types of objects as in Figure 3. The blue line ellipse indicates an approximate size of the Leo A galaxy—10' along the major axis. North is up and east is to the left.

important when performing observations at lower galactic latitudes.

For the identification of the early-type emission-line stars we employed the diagram  $NA-R$  versus  $B-V$  (Figure 3(b)), which is similar to the method used by Grebel (1997). Thirty-one probable Be-type or B[e]-type stars are marked with cyan dots. All these stars are located among the MS or blue-loop stars in the color-magnitude diagram (Figure 4) and are projected onto the central part of the Leo A galaxy (Figure 5). This supports their classification as Be or B[e] stars residing in the Leo A galaxy. Blue dots in Figure 3 mark 13 objects possessing a significant flux excess in the  $NA$  passband. These objects do not belong to the previous two groups of stars demonstrating extra flux in the  $NA$  passband (red and cyan dots in Figures 3–5).

## 5. Conclusions

We have surveyed the field ( $20' \times 24'$ ) surrounding the Local Group dwarf irregular galaxy Leo A in the  $R$  and  $NA$  ( $NA656$ ) passbands with the Subaru Telescope equipped with the Suprime-Cam mosaic camera. We employed the recently published ST photometric standards in the  $R$  passband and calibrated our observations. In this study, we present the photometry catalog of 28,224 objects, which supplements the published photometry data set of Leo A (Stonkutė et al. 2014). We believe it will be useful for the preparation of future imaging and spectroscopic observation programs.

We have demonstrated a capability of the  $NA-R$  color index to separate Milky Way M-type dwarfs and late-type evolved stars in external galaxies, as well as to identify early-type emission-line stars (Be, B[e]). It was shown that even the rather

wide (140 Å) *NA* passband is an efficient tool to perform object classification.

The bright ( $R < 23$  mag) starlike objects selected by applying narrow sharpness and  $\chi^2$  parameter ranges are plotted in Figures 3–5 and are marked in Table 1 as Type = 2. The identified 226 M-type dwarfs are evenly distributed across the field, which supports their classification as foreground stars. All 31 objects identified as early-type emission-line stars are concentrated at the center of Leo A, which supports their classification as Be-type or B[e]-type stars residing in the Leo A galaxy.

We thank the anonymous referee for constructive suggestions. We are grateful to Prof. P. B. Stetson for kindly providing the newest version of standard stars in the Leo A field. We are thankful to our collaborators: Nobuo Arimoto (P.I.), Takashi Hasegawa, Chisato Ikuta, Pascale Jablonka, Donatas Narbutis, Kouji Ohta, Naoyuki Tamura, Valdas Vansevicius, and Yoshihiko Yamada whose help at the stage of observations and preliminary data reduction was invaluable. The Leo A survey is based on Suprime-Cam images, collected at the Subaru Telescope, which is operated by the National Astronomical Observatory of Japan. The research has made use of the SAOImage DS9, developed by the Smithsonian Astrophysical Observatory, and the USNOFS Image and Catalog Archive operated by the United States Naval Observatory, Flagstaff Station.

*Facility:* The Subaru Telescope.

### ORCID iDs

Rima Stonkutė  <https://orcid.org/0000-0003-4987-2590>

Vladas Vansevicius  <https://orcid.org/0000-0002-3897-9504>

### References

- Brown, W. R., Geller, M. J., Kenyon, S. J., & Kurtz, M. J. 2007, *ApJ*, **666**, 231  
 Cole, A. A., Skillman, E. D., Tolstoy, E., et al. 2007, *ApJL*, **659**, L17  
 Dolphin, A. E., Saha, A., Claver, J., et al. 2002, *AJ*, **123**, 3154  
 Grebel, E. K. 1997, *A&A*, **317**, 448  
 Hunter, D. A., Ficut-Vicas, D., Ashley, T., et al. 2012, *AJ*, **144**, 134  
 Kirby, E. N., Rizzi, L., Held, E. V., et al. 2017, *ApJ*, **834**, 9  
 Leščinskaitė, A., Stonkutė, R., & Vansevicius, V. 2021, *A&A*, **647**, A170  
 Miyazaki, S., Komiyama, Y., Sekiguchi, M., et al. 2002, *PASJ*, **54**, 833  
 Pecaut, M. J., & Mamajek, E. E. 2013, *ApJS*, **208**, 9  
 Stetson, P. B. 1987, *PASP*, **99**, 191  
 Stetson, P. B. 2000, *PASP*, **112**, 925  
 Stetson, P. B., & Harris, W. E. 1988, *AJ*, **96**, 909  
 Stetson, P. B., Pancino, E., Zocchi, A., Sanna, N., & Monelli, M. 2019, *MNRAS*, **485**, 3042  
 Stonkutė, R., Arimoto, N., Hasegawa, T., et al. 2014, *ApJS*, **214**, 19  
 Stonkutė, R., Čeponis, M., Leščinskaitė, A., Naujalis, R., & Vansevicius, V. 2018, *A&A*, **614**, A144  
 Tody, D. 1993, in ASP Conf. Ser. 52, *Astronomical Data Analysis Software and Systems II*, ed. R. J. Hanisch et al. (San Francisco, CA: ASP), 173  
 Vansevicius, V., Arimoto, N., Hasegawa, T., et al. 2004, *ApJL*, **611**, L93